



# FRP-to-FRP bond characterization and force-based bond length model

Alaukik Singh\*, Enrique del Rey Castillo, Jason Ingham

Dept. of Civil and Environmental Engineering, The University of Auckland, New Zealand



## ARTICLE INFO

### Keywords:

FRP  
Strengthening  
Bond length  
Debonding  
FRP anchor  
FRP lap joint

## ABSTRACT

Fiber Reinforced Polymer (FRP) anchors are an effective method to increase the bond strength and/or ensure load path continuity between FRP materials and the concrete substrate when FRP materials are used as Externally Bonded Reinforcement (EBR) to strengthen and/or repair existing structures. While advances in developing a design methodology have been made on the fiber rupture and concrete cone failure modes for FRP anchors, the FRP-to-FRP bond behavior has received limited research attention. In an effort to develop design equations to calculate FRP-to-FRP bond capacity to be used by engineers, an extensive experimental program was undertaken to characterize the behavior of adhesively bonded FRP-to-FRP lap joints. Two force-based models to calculate the FRP-to-FRP bond capacity were proposed considering the influence of the critical bond length on lap joint behavior. A study to characterize the statistical properties of the experimental data was undertaken, and 95 and 99.87 percentile models were developed based on the statistical distribution of the experimental data set. Main conclusions inferred from the study and ideas for future work are also presented.

## 1. Introduction

Externally Bonded Fiber Reinforced Polymer (EBR-FRP) systems are widely used as a method for strengthening of existing structures. FRP materials feature a high strength to weight ratio, which is one of the main advantages of using FRP materials to improve the capacity of existing structures. FRP sheets, consisting of a varying number of fiber tows interweaved together, are one of the most commonly used products in EBR-FRP systems. The sheets are saturated with epoxy resins to form a composite matrix and then adhered to the external surface of the structure, but premature debonding of the FRP sheets from the concrete substrate is one of the main drawbacks of EBR-FRP systems [1]. Another common problem is the obstructions caused by structural or non-structural elements that prevent the complete wrapping of the structure. Both of these problems limit the FRP design strain that the engineers can use when implementing EBR-FRP systems.

The use of FRP anchors has been identified as one possible method to minimize premature FRP-to-concrete debonding [2,3], by transferring load from the FRP sheet directly into the RC structure. FRP anchors (as shown in Fig. 1 [4]) consist of a bundle of fibers splayed in a fan shape and bonded onto the FRP sheet at one end, with the bundle of fibers being embedded into the structure at the other end. FRP anchors typically feature a high concentration of stresses at the section where the fan transitions into the dowel, commonly known as the key portion of the anchor.

The lack of a design methodology for FRP anchors is the main impediment to their widespread use [2], although initial efforts have been made to study the failure modes of FRP anchors. Studies can be found in literature regarding the concrete cone failure mode [5] and fiber rupture failure mode of FRP anchors [6], even considering nonlinearity of fibers and concentration of stresses [7]. By contrast, the fan-to-sheet failure mode has received limited research attention, and is simply the debond failure between the anchor fan and the FRP sheet to which is bonded. The fan-to-sheet failure mode can be assimilated to a simple case of two fiber sheets debonding as a result of excessive shear load on the FRP-to-FRP interface. The FRP-to-FRP bond behavior has been studied by several researchers for different curing conditions [8,9], and several adhesive failure-based stress models [10,11] for composite (such as FRP-to-steel) lap joints have been developed. However, a model with simple design equations that can be readily used by engineers to calculate the design capacity of FRP-to-FRP bond was not found. With reference to the fan-to-sheet failure in FRP anchors, a project was undertaken by Kanitkar [12] with the aim being to develop a simplified design equation to calculate the fan-to-sheet bond capacity to be used by an engineer. In the model developed by Kanitkar the shear strength of the resin is the governing parameter in the equation, but unfortunately this parameter is typically not available to engineers, which compromises the applicability of the equation. Additionally, the limited number of specimens tested and the lack of consistency observed in the failure modes compromises the reliability of the findings.

\* Corresponding author.

E-mail address: [singh\\_alaukik@berkeley.edu](mailto:singh_alaukik@berkeley.edu) (A. Singh).

**Nomenclature**

*Appendix Notation*

$A_w$	lap joint measured bond area in mm <sup>2</sup>
CoV	coefficient of variation in %
$C_{c1}$ to $C_{c4}$	calibration factors for the developed FRP-to-FRP debond capacity
$E_f$	elastic modulus of FRP in the direction of the fiber in N/mm <sup>2</sup>
$E_r$	elastic modulus of the resin in N/mm <sup>2</sup>
FC	factor of confidence
$G_r$	shear fracture energy of debonding between fiber and resin in N/mm <sup>2</sup>
$L$	bond length in mm
$L_{cr}$	critical bond length in mm
$L_n$	normalized bond length in mm
$L_m$	measured bond length in mm
$L_t$	target bond length in mm
$\bar{N}_{bond}$	calculate average debonding load capacity for a given lap joint in kN
$\bar{N}_{bond}^{95\%}$	calculate 95 percentile debonding load capacity for a given lap joint in kN

$\bar{N}_{bond}^{99.87\%}$	calculate 99.87 percentile debonding load capacity for a given lap joint in kN
$P$	measured debonding load in kN
$\bar{P}$	average measured debonding load for a group of tests in kN
$SD$	standard deviation in kN
$S_u$	fiber deformability matrix component equal to 0.25 mm
$W_m$	lap joint measured width in mm
$b$	width of the concrete section in mm
$b_f$	width of the FRP sheet in mm
$f_{bd}$	design FRP-to-concrete bond strength in N/mm <sup>2</sup>
$f_{cm}$	concrete compressive strength in N/mm <sup>2</sup>
$f_{ctm}$	concrete tensile strength in N/mm <sup>2</sup>
$f_{fd}$	design FRP-to-FRP bond strength in N/mm <sup>2</sup>
$k_b$	geometrical corrective factor
$k_g$	corrective factor
$t_f$	thickness of fiber sheet in mm
$\Gamma$	design specific fracture energy in N/mm <sup>2</sup>
$\gamma_{RD}$	corrective factor equal to 1.25
$\sigma_f$	tensile strength of the FRP in N/mm <sup>2</sup>
$\sigma_r$	tensile strength of the resin in N/mm <sup>2</sup> and
$\tau_r$	shear strength of the resin in N/mm <sup>2</sup> .

Due to a lack of literature regarding FRP-to-FRP bond behavior, widely studied and accepted FRP-to-concrete literature can be used to understand the FRP-to-FRP bond behavior. Chen and Teng [13] investigated FRP-to-concrete bond behavior and observed that the load applied to an FRP sheet bonded to concrete was linearly correlated to the bond area up to a certain limit, with the bond area being equal to the effective bond length multiplied by the width of the FRP-to-concrete interface. Beyond that limit, which was defined as the effective bond length (hereafter referred to as the critical bond length), the applied load did not increase, although a more ductile response could be achieved because the debonding process spanned for a longer period of time. This behavior has since been observed in many studies and adopted in international design guidelines such as ACI 440 [14] and

CNR-DT-200 [15]. A similar behavior is expected to occur at the FRP-to-FRP interface but a comprehensive study of FRP-to-FRP behavior is paramount to verify the presence of a critical bond length in FRP-to-FRP joints and to develop an associated description of the bond behavior. Therefore, 30 FRP-to-FRP coupons with a single bonding surface (single lap joints) and 25 FRP-to-FRP coupons with two bonding surfaces (double lap joints) were tested until debonding occurred, with the objective being to characterize the FRP-to-FRP critical bond length and associated bond behavior. It should be noted that the reported study represented a trial effort to investigate the FRP-to-FRP bond behavior and that further verification of the test results with FRP anchors as used in a realistic application such as strengthening of columns [16] is necessary before a correlation between FRP coupons and FRP anchors can be established.

**2. Experimental program**

The material properties, the test matrix, the preparation of the specimen and the testing set-up are described in detail in this section.

**2.1. Materials**

Unidirectional carbon fiber sheets [17] and the corresponding impregnating epoxy resin [18] were used throughout the experimental program. The physical and mechanical properties of both cured laminate and impregnating resin are reported in Table 1, where all the material properties specified are as provided by the manufacturers.

**2.2. Test matrix**

The experimental program was designed following the approach that bond length was the only varying parameter while all other parameters were maintained constant to determine the critical length for both single and double FRP-to-FRP lap joints. All the dimensions were in accordance with ASTM D5868 [22] and ASTM D3528 [23] for single and double lap joints respectively, as shown in Fig. 2. Five specimens for each bond length and a constant width of 25 mm of both single and double lap joints were tested, with the nomenclature being reported in Table 2. For example 1S represents a single bonding surface and 25a-25e represents the five specimens tested with a bond length of

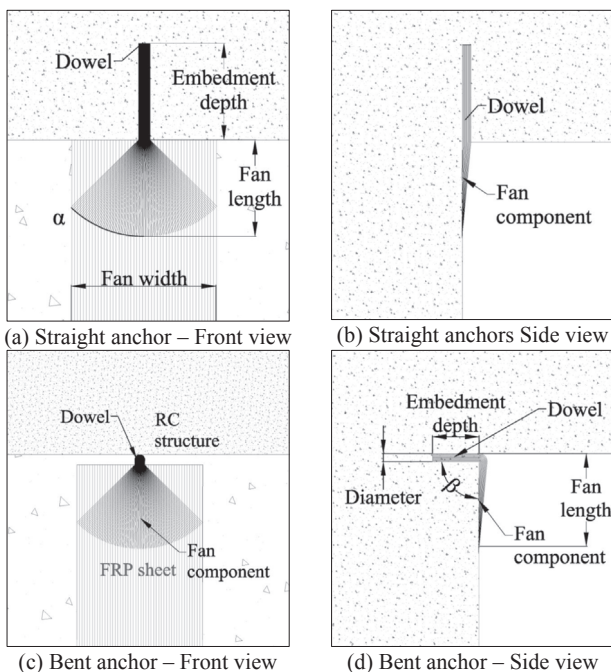


Fig. 1. Attributes of FRP anchors [4].

**Table 1**  
Material properties

Cured laminate properties of FRP sheet <sup>†</sup>		Mechanical properties of resin <sup>‡</sup>	
Laminate thickness	1.0 mm	Average flexural modulus	2.8 GPa
Average tensile modulus	75.7 GPa	Average tensile modulus	3.5 GPa
Average tensile strength	968 MPa	Average tensile strength	45 MPa
Rupture strain	1.0%	Rupture strain	1.5%

<sup>‡</sup> The resin properties were obtained after a 7 days curing period at 23°C. Average flexural modulus value based on testing carried out in accordance with ASTM D790 [20], whereas average tensile modulus, tensile strength and rupture strain were obtained in accordance with ASTM D638 [21].

<sup>†</sup> Values obtained in the longitudinal direction of the fibres in accordance with ASTM D3039 [19]

25 mm.

### 2.3. Specimen preparation

A preliminary study of the effect of curing time on resin strength in accordance to ASTM D638 was undertaken, with the results being reported in Fig. 3. No significant variation of tensile capacity was observed in the resin after three days curing, with the average strength being 34.2 MPa. Hence, the curing period for all the specimens was set at a minimum of three days to accelerate the testing program.

The first step in the preparation of test coupons was to cut two small rectangular sheets from a larger FRP fabric roll and soak the sheets in impregnating epoxy resin. Then a specific lap splice length (or bond length) was targeted for bonding the two sheets. For example, for the 1S-25 specimens the target bond length was 25 mm while bonding the two FRP sheets. The bonded sheets were designed to provide five FRP-to-FRP bonded coupons, each having a width equal to 25 mm with a specific bond length (25 mm in the 1S-25 example). Similarly, for the double lap joints an extra sheet was bonded using the same target length. For example, for the 2S-25 specimen, two bonding surfaces with a 25 mm overlap was targeted. With the entire specimen preparation process being manual, actual bond lengths differed slightly from the intended bond lengths. The use of thicker tabs at the ends of the specimens was deemed unnecessary, as the debond failure mode was predominant over fibre rupture failure mode. An environmental chamber (Contherm Biosyn series Model 6800CP8- 800Lt) maintained at 23 degrees Celsius and 50% relative humidity was used for curing all the specimens, as well as eight resin coupons to correlate the test results with the resin strength. After at least three days of curing, the FRP-to-FRP bonded sheet was removed from the chamber and cut into five coupons, each being 25 mm wide, by using a hand-held electric cutter and a cutting guide built specifically for this purpose. An average deviation of 5.9% from the targeted 25 mm width of the coupons was observed despite the cutting being mechanized and guided. A speckle pattern for measuring displacements and strains using the Digital Image Correlation technique was prepared on the FRP coupons by painting the cured sheet in two layers, the first one being a black matte layer and the

second layer being white sprayed dots. After the paint dried, the specimens were ready for testing.

### 2.4. Test set-up

An Instron 50 kN and an Instron 100 kN universal testing machines were used to test the coupons following the loading protocol from ASTM D5868 [24], which recommends a constant ramp rate of 2 mm/min. As reported in Fig. 4, a pair of DSLR cameras, together with artificial white lights, were installed in front of the specimen to record displacements and strains using the Digital Image Correlation (DIC) technique.

## 3. Results

The peak load, recorded when the FRP-to-FRP debonding occurred and therefore referred to hereafter as the debonding load, is reported in Table 3 for all the specimens, together with the measured bond length and specimen width. Because the actual width of the specimens differed slightly from the targeted 25 mm, the bond lengths had to be normalized according to the actual width. To normalize the bond length, the bond area of the coupon measured post-test was divided by the nominal width (25 mm) as per ASTM D5868 [22].

### 3.1. Critical length

The debonding load for all the tested coupons is plotted against the normalized bond lengths using non-linear least squares curve fitting method in Fig. 5. The debonding load increased linearly with respect to the bond length until a certain length, after which no significant change in load was observed, as can be seen in Fig. 5. This behavior confirmed the hypothesis that a critical bond length (or critical bond area) exists, with the behavior of both single and double lap joint specimens being in accordance with this hypothesis. The effective bond length of double lap joint specimens was observed to be larger than that of single lap joint specimens, with the debonding load of double lap joints being almost double the debonding load of single lap joints when the bond length surpassed the effective bond length.

### 3.2. Strain patterns

The photographs acquired during the tension test described in Section 3 were processed using a Matlab [25] GUI, MODEM [26,27], developed by the Centre for Advanced Composite Materials (CACM) at the University of Auckland. Fig. 6 shows the strain variations on the FRP surface, with the strain variations along both the transverse and longitudinal direction being depicted according to the strain % ranging from -2% to 2%. The regions with high tensile strains are represented by a red colour, while the regions with high compressive strains are represented by a blue colour. A concentration of tensile strains in the longitudinal direction of the FRP fibers was observed at the end of the lap area, with the strains in the lap area being significantly lower than

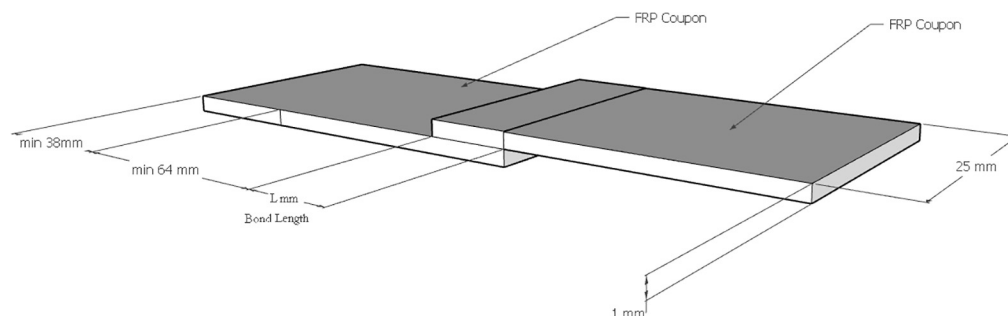


**Fig. 2.** Specimen dimensions according to ASTM D3528 [23].

**Table 2**  
Test matrix.

Single lap joints			Double lap joints		
Bond length (mm)	No of surfaces	Coupon name	Bond length (mm)	No of surfaces	Coupon name
25	1	1S25a to 1S25e	10	2	2S10a to 2S10e
37.5	1	1S37.5a to 1S37.5e	25	2	2S25a to 2S25e
50	1	1S50a to 1S50e	50	2	2S50a to 2S50e
62.5	1	1S62.5a to 1S62.5e	75	2	2S75a to 2S75e
75	1	1S75a to 1S75e	100	2	2S100a to 2S100e
100	1	1S100a to 1S100e			

Total of 55 specimens

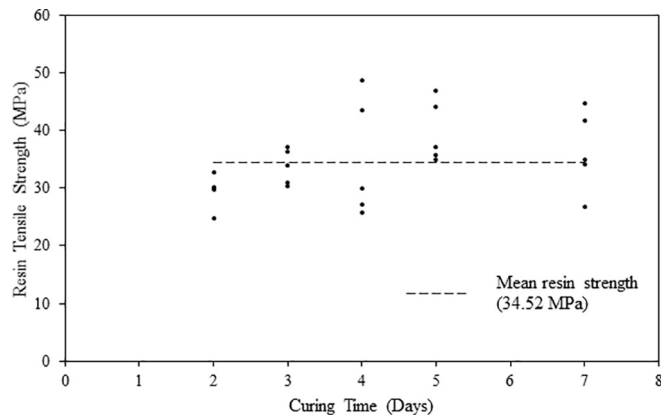


Fig. 3. Effect of curing time on resin strength in using ASTM D638 [21].

the strains at the end of the overlapping area. The reason for the low strains observed in the bonded area was attributed to the presence of two overlaying FRP sheets instead of a single sheet, which resulted in doubling of the cross sectional area of the coupon in the bonded region when compared with the rest of the coupon. The compression strains observed in the transverse direction were in accordance with the influence of the Poisson effect, which resulted in a reduction of transverse width (compression) as a consequence of an increment in longitudinal length (tension) originating from the tensile load applied to the coupons.

3.3. Failure mode

A thin layer of resin between the FRP sheets constituted the FRP-to-FRP bond. Only minimum damage was observed in the FRP sheets after testing, which indicated shear failure of the resin layer between the two FRP sheets. The FRP-to-FRP debonding failure observed for the test coupons was sudden and brittle, without any preliminary signs of failure in the coupons. This behavior was observed to be consistent for all bond lengths with both single and double lap joints, indicating that neither an increase in bond length nor an additional bonding surface (as for the case of double lap joints) affected the ductility of the bond area and the debonding failure mode.

4. Design models

Multiple models have been proposed to characterize the behavior of adhesively bonded joints, with da Silva having compiled a comprehensive review and concluded that the bond strength and behavior of lap joints with different materials cannot be characterized adequately by a single model, and that different models for different materials are required [28]. The observed relationship between debonding load and bond length when testing FRP-to-FRP coupons is summarized in Fig. 5 and corresponds with previously reported metal-to-metal bond

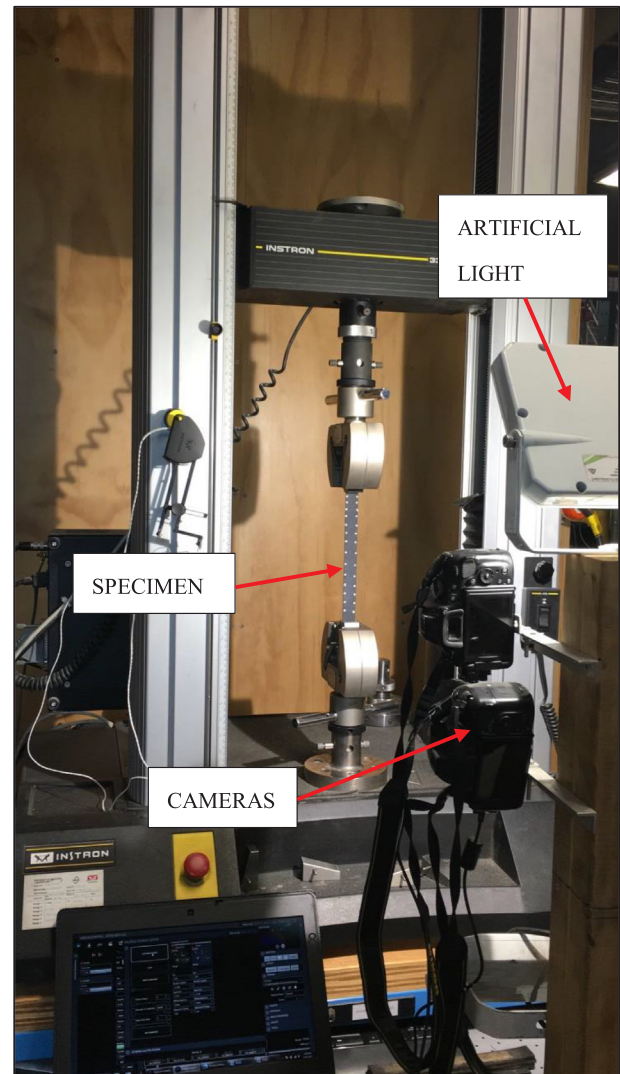


Fig. 4. Effect of anchor properties on fiber rupture strength of straight anchors.

behavior [29] and with previously reported FRP-to-concrete bond behavior [13]. However, a model based on critical bond length for FRP-to-FRP bond behavior has not previously been reported, emphasizing the need for a simple model that is suitable for use by practicing engineers. Therefore, accepted FRP-to-concrete models [30,13,15] were adapted for FRP-to-FRP bond to develop design equations consistent with the results summarized in Table 3.

**Table 3**  
Debonding loads for both single and double lap joints.

Specimen name	Target length $L_t$ (mm)	Measured length $L_m$ (mm)	Measured width $W_m$ (mm)	Measured area $A_m$ (mm <sup>2</sup> )	Normalized length $L_n$ (mm)	Load P (kN)
1S25a	25	20.4	23.5	480.0	19.2	11.5
1S25b	25	23.1	25.2	580.3	17.7	11.7
1S25c	25	27.3	25.2	688.6	27.5	13.5
1S25d	25	27.0	26.7	718.9	28.8	13.6
1S25e	25	22.9	27.7	633.8	25.4	13.4
1S37.5a	37.5	42.9	22.2	950.5	38.0	21.5
1S37.5b	37.5	40.3	22.4	904.0	36.1	11.6
1S37.5c	37.5	39.1	22.5	882.3	35.2	13.8
1S37.5d	37.5	40.4	23.2	937.7	37.5	22.6
1S37.5e	370.5	41.4	22.4	926.3	37.0	14.3
1S50a	50	48.5	24.5	1188.41	47.5	23.3
1S50b	50	52.0	24.9	1294.5	51.7	27.8
1S50c	50	48.9	25.0	1221.9	48.8	20.9
1S50d	50	50.6	25.1	1266.9	50.6	27.2
1S50e	50	50.2	24.8	1244.0	49.7	26.2
1S62.5a	62.5	63.4	22.6	1430.6	57.2	21.8
1S62.5b	62.5	62.2	22.7	1410.3	56.4	31.8
1S62.5c	62.5	62.9	22.7	1429.5	57.1	19.1
1S62.5d	62.5	63.2	22.2	1402.7	56.1	21.1
1S62.5e	62.5	62.8	22.4	1406.2	56.2	23.9
1S75a	75	76.0	24.2	1834.6	73.3	26.7
1S75b	75	75.6	23.2	1755.0	70.2	27.3
1S75c	75	75.6	24.3	1835.5	73.4	25.6
1S75d	75	75.4	23.9	1800.8	72.0	26.6
1S75e	75	75.3	24.4	1834.7	73.3	33.8
1S100a	100	103.3	24.7	2552.8	102.1	28.2
1S100b	100	100.5	22.8	2292.3	91.6	25.6
1S100c	100	103.5	24.1	2495.5	99.8	31.9
1S100d	100	100.7	23.7	2383.6	95.3	28.6
1S100e	100	100.0	22.5	2254.2	90.1	27.0

Specimen name	Target length $L_t$ (mm)	Measured length $L_m$ (mm)	Measured width $W_m$ (mm)	Measured area $A_m$ (mm <sup>2</sup> )	Normalized length $L_n$ (mm)	Load N (kN)
2S10a	10	16.5	19.2	315.8	12.6	14.0
2S10b	10	15.9	20.5	325.8	13.0	16.6
2S10c	10	15.6	22.5	349.9	14.0	16.8
2S10d	10	15.2	19.3	293.2	11.7	12.5
2S10e	10	15.8	20.1	316.0	12.6	12.5
2S25a	25	25.5	23.5	601.1	24.0	17.5
2S25b	25	26.2	24.1	629.7	25.1	18.7
2S25c	25	25.9	23.6	610.7	24.4	20.7
2S25d	25	25.5	24.0	611.9	24.4	17.4
2S25e	25	26.3	23.8	624.7	25.0	21.8
2S50a	50	54.0	22.8	1230.0	49.2	31.1
2S50b	50	53.0	22.8	1208.9	48.3	30.0
2S50c	50	53.1	22.8	1211.6	48.4	29.6
2S50d	50	51.7	22.7	1171.1	46.8	34.2
2S50e	50	54.0	23.2	1250.1	50.0	30.6
2S75a	75	73.6	26.0	1914.3	76.5	50.6
2S75b	75	75.8	25.8	1952.5	78.1	59.0
2S75c	75	80.0	25.1	2005.3	80.2	45.2
2S75d	75	76.9	24.7	1899.4	75.9	55.8
2S75e	75	71.8	25.2	1812.0	72.4	46.6
2S100a	100	104.3	25.9	2698.4	107.9	48.8
2S100b	100	103.8	23.1	2398.0	95.9	55.0
2S100c	100	102.9	26.1	2686.7	107.4	55.0
2S100d	100	106.7	25.6	2736.8	109.4	57.9
2S100e	100	104.2	26.2	2733.1	109.3	56.6

\*The targeted width was 25 mm in all cases.

### 4.1. Fracture energy model

The fracture energy model was based on the principle that bond failure occurs only if the rate of applied energy is greater than a critical fracture energy rate. The strength model for FRP-to-concrete bond developed by Chen and Teng [13] is a widely accepted model that has

been adopted by CNR-DT 200 [15], and was used as the basis of the present study to provide a fracture energy model for FRP-to-FRP bond behavior. CNR [15] defines the fracture energy for the FRP-concrete interface (reported in Eq. (1)) to be dependent on the concrete compressive strength ( $f_{cm}$ ) and concrete tensile strength ( $f_{ctm}$ ), as well as a geometrical corrective factor ( $k_b$ ):

$$\Gamma = \frac{k_b k_g}{FC} f_{cm} f_{ctm} \tag{1}$$

Where  $\Gamma$  is the design specific fracture energy in N/mm,  $k_b$  is a geometrical corrective factor defined in Eq. (2),  $k_g$  is an additional corrective factor (0.023 mm for pre-cured lay-up and 0.037 mm for wet lay-up),  $f_{cm}$  is the mean compressive strength of concrete in N/mm<sup>2</sup>,  $f_{ctm}$  is the mean tensile strength of concrete in N/mm<sup>2</sup>, and FC is the confidence factor.

$$k_b = \sqrt{\frac{2 - b_f/b}{1 + b_f/b}} \tag{2}$$

where  $b_f$  is the width of fiber sheet in mm and  $b$  is the width of concrete section in mm.

CNR [15] defines the optimal (or critical) bond length as the length which when exceeded does not lead to any increase in the force transferred between concrete and FRP. This critical length, given in Eq. (3), is proportional to the elastic modulus ( $E_f$ ) and thickness ( $t_f$ ) of FRP coupon and the fracture energy of the concrete-to-FRP bond ( $\Gamma$ ).

$$L_{cr} = \frac{1}{\gamma_{Rd} f_{bd}} \sqrt{\frac{\pi^2 E_f t_f \Gamma}{2}} \tag{3}$$

Where  $L_{cr}$  is critical bond length in mm,  $\gamma_{Rd}$  is a corrective factor equal to 1.25,  $f_{bd}$  is the design bond strength between FRP and concrete in N/mm<sup>2</sup> as defined by Eq. (4),  $E_f$  is the elastic modulus for FRP in the direction of force in N/mm<sup>2</sup>,  $t_f$  is the thickness of each cured FRP sheet in mm,  $\Gamma$  is the design value of specific fracture energy for FRP-to-concrete bond in N/mm.

$$f_{bd} = \frac{2\Gamma}{S_u} \tag{4}$$

Where  $S_u$  is the fiber deformability matrix component and is equal to 0.25 mm

Finally, using the critical length from Eq. (3) and the fracture energy from Eq. (1), the debonding load capacity of concrete-to-FRP bond as given by CNR [15] can be calculated using Eq. (5).

$$P = \begin{cases} \frac{b_f}{\gamma_{fd}} \sqrt{2\Gamma E_f t_f} \frac{L}{L_{cr}} \left(2 - \frac{L}{L_{cr}}\right) & L < L_{cr} \\ \frac{b_f}{\gamma_{fd}} \sqrt{2\Gamma E_f t_f} & L \geq L_{cr} \end{cases} \tag{5}$$

As inferred from Eq. (1), the concrete compressive and tensile strengths are the governing parameters for fracture energy at the FRP-to-concrete interface because concrete is the weaker material governing bond failure. Similarly, the adhesive (in this case epoxy resin) used to bond the FRP sheets is the material dictating the characteristics of the FRP-to-FRP bond. Therefore, for an effective adaptation of the FRP-to-concrete bond model described in CNR [15] into a fracture energy model for FRP-to-FRP bond, the fracture energy necessary for the FRP-to-resin interface to fail should be specified instead of the fracture energy associated with failure of the FRP-to-concrete interface. The model by Outwater and Murphy [31], already available in the literature, can be used to specify the FRP-to-resin interface shear failure strength given by Eq. (6). Outwater and Murphy [31] defined the FRP-to-resin interface shear failure strength to be dependent on the tensile strength ( $\sigma_r$ ) and the elastic modulus ( $E_r$ ) of the resin, being the material dictating the characteristics of the FRP-to-FRP bond. This assumption directly correlates with the failure mode observed in FRP coupons as discussed in Section 3.3, and also relates the fracture energy to the characteristics of

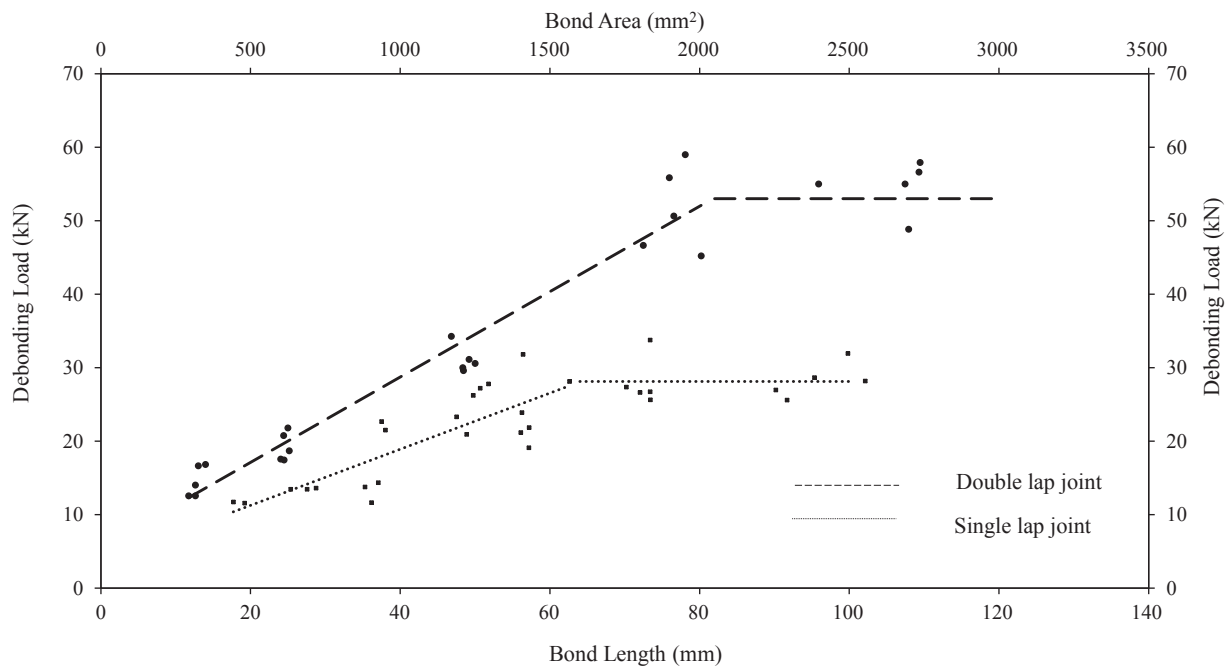


Fig. 5. Double bonding surface vs single bonding surface.

the weaker material.

$$G_r = \frac{\sigma_r^2 E_f b_f}{8E_r^2} \tag{6}$$

Where  $G_r$  is the shear fracture energy of debonding between fiber and resin in N/mm,  $\sigma_r$  is the manufacturer tensile strength of resin in N/mm<sup>2</sup>,  $E_r$  is the elastic modulus for the resin in N/mm<sup>2</sup>,  $b_f$  is the diameter

of the filament in mm (in this experimental program,  $b_f$  is the width of the fiber coupon).

The critical length for FRP-to-FRP bond can be calculated using Eq. (7) by adapting the fracture energy equation from Outwater and Murphy [31] and introducing a coefficient ( $C_{cl}$ ) to calibrate the original expression using the experimental data.

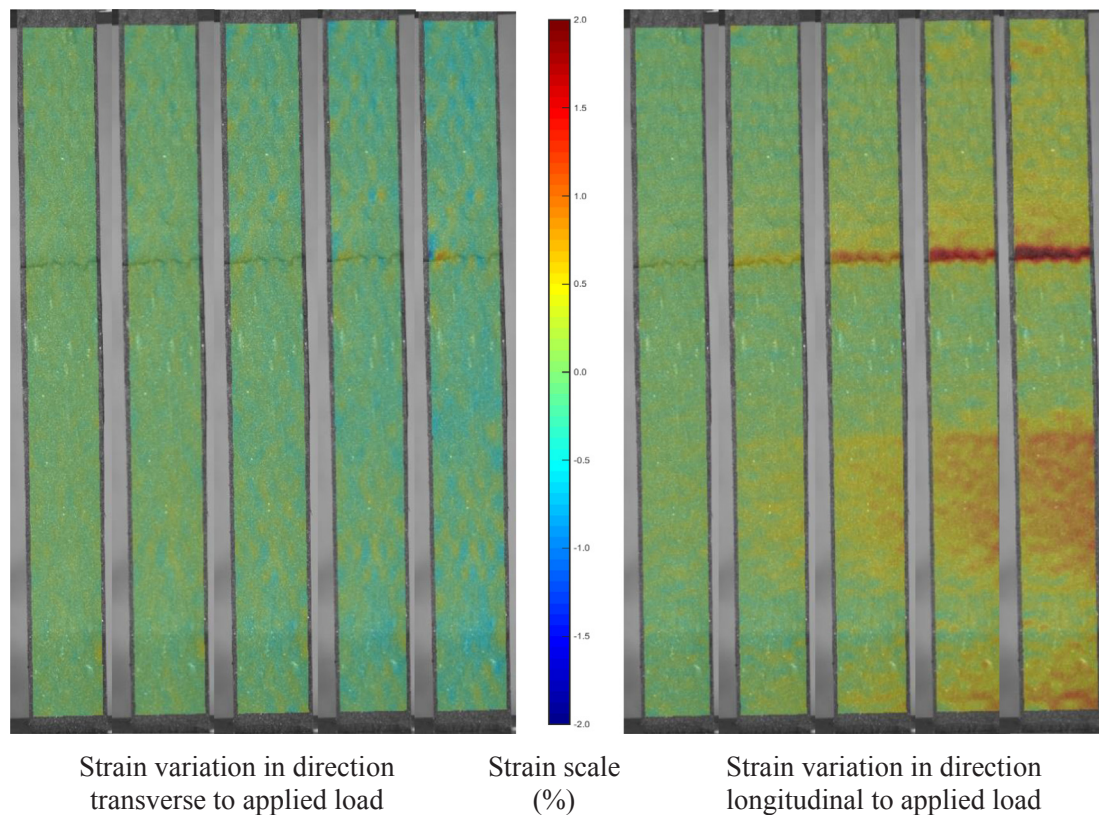


Fig. 6. Strain variation in FRP coupons tested according to ASTM D5868 [22].

$$L_{cr} = \frac{1}{C_{c1}f_{fd}} \sqrt{\frac{\pi^2 E_f t_f G_r}{2}} \tag{7}$$

Where  $f_{fd}$  is the design FRP-to-FRP strength in N/mm<sup>2</sup> and is equal to  $2G_r/S_u$ .

Similar to the approach from CNR [15], the expression for the FRP-to-FRP debonding load can be derived by using the fracture energy and critical length equations given in Eqs. (6) and (7) respectively. Therefore the FRP-to-FRP bond capacity for different bond lengths can be given by Eq. (8) with a calibration factor ( $C_{c2}$ ), similar to the one in Eq. (7), being incorporated into the expression.

$$\bar{N}_{bond} = \begin{cases} C_{c2} b_f \sqrt{2G_r E_f t_f} \frac{L}{L_{cr}} & L < L_{cr} \\ C_{c2} b_f \sqrt{2G_r E_f t_f} & L \geq L_{cr} \end{cases} \tag{8}$$

Where  $\bar{N}_{bond}$  is the maximum load capacity for the lap joint for a given bond length in kN.

The factors  $C_{c1}$  and  $C_{c2}$  in design equations Eqs. (7) and (8) respectively were calibrated with the test results given in Table 3 using the non-linear least squares curve fitting method with 95% confidence bounds. The ratio between the model value and the experimental value was 0.95, with a coefficient of variation of 17.7%. The final equation with the calibration coefficients required to calculate the average capacity of FRP-to-FRP single lap joints exhibiting the debonding failure mode are reported in Eqs. (9) and (10).

$$\bar{N}_{bond} = \begin{cases} 0.33 b_f \sqrt{2G_r E_f t_f} \frac{L}{L_{cr}} & L < L_{cr} \\ 0.33 b_f \sqrt{2G_r E_f t_f} & L \geq L_{cr} \end{cases} \tag{9}$$

$$L_{cr} = \frac{1}{0.30 f_{fd}} \sqrt{\frac{\pi^2 E_f t_f G_r}{2}} \tag{10}$$

Similarly, the design equations for the double lap joints is given by Eqs. (11) and (12)

$$\bar{N}_{bond} = \begin{cases} 0.63 b_f \sqrt{2G_r E_f t_f} \frac{L}{L_{cr}} & L < L_{cr} \\ 0.63 b_f \sqrt{2G_r E_f t_f} & L \geq L_{cr} \end{cases} \tag{11}$$

$$L_{cr} = \frac{1}{0.20 f_{fd}} \sqrt{\frac{\pi^2 E_f t_f G_r}{2}} \tag{12}$$

#### 4.2. Modified Adams model

Despite the comprehensive nature of the fracture energy model described in the previous section, the complexity of the model may compromise the applicability by practicing engineers. In order to reduce this complexity, the Adams et al. [32] model was used instead, which defines the lap joint behavior depending on the adhesive and the adherend property while also considering a critical bond length. For lap joints, adherend is defined as any substance bonded to another by an adhesive. For example, epoxy resin was the adhesive while the FRP sheet was the adherend for the FRP-to-FRP lap joints investigated in the reported experimental program (as described in Section 2). Most of the models found in the literature [10,33,11] assume adhesive failure to be the governing factor for debonding failure in the case of composite joints (such as the FRP-to-FRP joints investigated herein). However, Adams [32] hypothesized yielding of the adherend to be a limit factor for the bond strength, instead of adhesive failure, but only after a certain point. The Adams model [32], graphically represented in Fig. 7, assumes a pure adhesive failure when the bond length to thickness ratio ( $L/t$ ) is less than 20. Once the  $L/t$  ratio exceeds 20, adherend yielding instead of adhesive failure governs the bond load capacity. For the FRP-to-FRP bonded test coupons under study, FRP sheet (adherend) failure was not observed, which is in disagreement with Adams' assumption of

adherend failure limiting the bond strength of adhesively bonded joints. However, the results reported in Table 3 and the corresponding regression curve reported in Fig. 5 indicated a bond behavior similar to the Adams model reported in Fig. 7. Therefore, an approach similar to the approach followed by Adams et al. [32] was adopted to develop simple design equations for FRP-to-FRP adhesively bonded joints, with the epoxy resin being the adhesive (the resin properties are reported in Table 1).

Similar to the approach followed by Adams et al. [32], a pure adhesive failure in FRP-to-FRP specimens was assumed for short bond length, but as the bond length increased the assumed adherend failure (FRP sheet) governed the bond capacity instead of adhesive failure (Point B in Fig. 8). Adhesive failure was assumed from point A to point B and fiber failure was assumed to limit any increase in FRP-to-FRP bond capacity beyond point B, despite increasing the bond length. The bilinear curve ABC in Fig. 8 represents the variation of FRP-to-FRP bond capacity.

In the modified Adams model, the FRP-to-FRP bond capacity is initially assumed to increase linearly with bond length, represented by AB in Fig. 8 (adhesive failure). After a certain bond length, the FRP sheet was assumed to fail instead of the adhesive, causing the bond to fail in shear. Hence the bond length at which the fiber fails instead of the adhesive is referred to as the critical bond length. This definition is adopted because beyond that length, any increase in bond length would have no effect on the debonding load as the fiber will still fail at the same load. The linear variation AB in Fig. 8 corresponding to pure adhesive failure is directly proportional to the adhesive (epoxy resin) strength and bond length and can be specified as Eq. (13)

$$P = \tau_r b_f L \text{ for } L < L_{cr} \tag{13}$$

Where  $\tau_r$  is the shear strength of resin in N/mm<sup>2</sup>.

However, the shear strength of the resin is not usually provided by manufacturers, and hence the typically provided value of resin tensile strength ( $\sigma_r$ ) was used to specify the adhesive failure. A calibration coefficient  $C_{c3}$ , calculated from the experimental results reported in Table 3, was introduced in order to adjust Eqs. (13) to form (14).

$$\bar{N}_{bond} = C_{c3} \sigma_r b_f L \text{ for } L < L_{cr} \tag{14}$$

Where  $\sigma_r$  is the resin tensile strength in N/mm<sup>2</sup>,  $L_f$ , and  $L$  is the overlap length of the bond in mm.

The bond capacity for the case of a pure adhesive failure is specified in Eq. (14) but, similar to Adams' approach, the adherend (the FRP sheet in this study) was hypothesized to contribute to the debonding behavior and hence limit the debonding load to the rupture capacity of the FRP sheet. Therefore, the FRP-to-FRP bond capacity (based on rupture capacity of the fibers) for bond lengths greater than the critical bond lengths can be specified using Eq. (15). A calibration coefficient ( $C_{c4}$ ) was introduced to correlate the FRP-to-FRP bond capacity data with the FRP tensile strength.

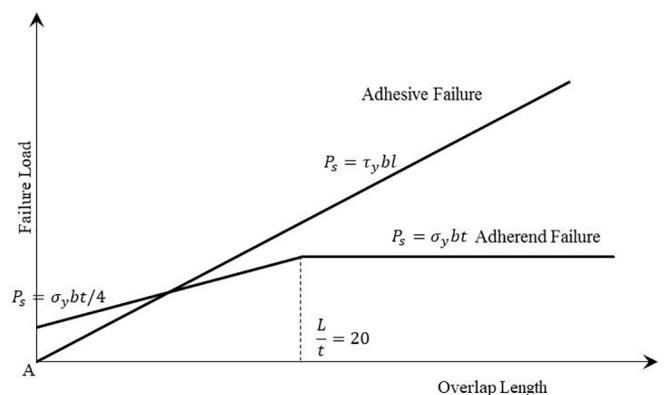


Fig. 7. Adams model for adhesively bonded joint failure.

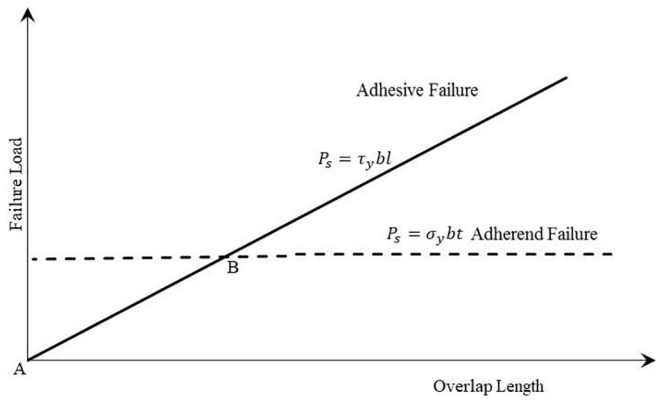


Fig. 8. Adams modified mode.

$$\bar{N}_{bond} = C_{c4} \sigma_f b_f t_f \text{ for } L \geq L_{cr} \tag{15}$$

Where  $\sigma_f$  is the FRP tensile strength in N/mm<sup>2</sup>.

Eq. (14) and Eq. (15) were calibrated with the test results given in Table 3 using the non-linear least squares curve fitting method with 95% confidence bounds. The average ratio of the model value to experimental value was 0.95 with a coefficient of variation of 27.25%. The final equation with the calibration coefficient required to calculate the average capacity of FRP-to-FRP bond capacity of single lap joints is given by equations Eqs. (16) and Eq. (17).

$$\bar{N}_{bond} = \begin{cases} \bar{N}_{bond} = 0.4\sigma_f b_f L & L < L_{cr} \\ \bar{N}_{bond} = 0.6\sigma_f b_f t_f & L \geq L_{cr} \end{cases} \tag{16}$$

$$L_{cr} = \frac{3\sigma_f t_f}{2\sigma_r} \tag{17}$$

Similarly for double lap joints, the design equations are given by Eqs. (18) and (19).

$$\bar{N}_{bond} = \begin{cases} \bar{N}_{bond} = 0.6\sigma_r b_f L & L < L_{cr} \\ \bar{N}_{bond} = 1.2\sigma_f b_f t_f & L \geq L_{cr} \end{cases} \tag{18}$$

$$L_{cr} = \frac{2\sigma_f t_f}{\sigma_r} \tag{19}$$

#### 4.3. Comparative study between the two models

A comparative study between the two proposed models was undertaken to assess and compare the effectiveness of the two models. The smaller coefficient of variation of the fracture energy model (17.70%) compared to the modified Adams model (27.25%) renders the fracture energy model more accurate than the modified Adams model. A comparison between the experimental debonding load and the predicted debonding load for both the fracture energy model and the modified Adams model is reported in Fig. 9. Both models were found to have a good correlation between the experimental and the predicted data sets, with an  $r^2$  value of 0.99 and 0.95 for the fracture energy model and the modified Adams model respectively. While the fracture energy model provides a more complex and detailed characterization of the FRP-to-FRP bond behavior and load capacity, the modified Adams model provides simple, easy to use design equations albeit with a lower accuracy than for the fracture energy model.

#### 4.4. Characteristic values

Safety factors are typically used in engineering design to provide further assurance to engineers regarding the reliability of a design. One example of such safety measures is the use of 99.87 and 95 percentile values, with these values being dependant on the statistical distribution

and the standard deviation (SD) of the test results. The average debonding load, standard deviation, and coefficient of variation for each set of specimens with the same targeted bond length have been reported in Table 4. The standard deviations for single lap joint specimens with bond lengths of 37.5 mm and 62.5 mm were uncharacteristically high, rendering them to be outliers. Hence, the standard deviation for these bond lengths was assumed to be the average of the standard deviations for the rest of the specimens while calculating the final equations with 99.87 and 95 correction factors.

The debonding loads for single lap joints reported in Table 3 were normalized by dividing the debonding loads by the average debonding load for the specimens with the same targeted bond length, with the normalized data being reported in Table 5. For example, the debonding loads for 1S-25 specimens were normalized by dividing each of the five debonding loads by the average debonding load of the five specimens. The normalized data was tested for a normal distribution by using the most common normality tests i.e. the Kolmogorov-Smirnov (K-S) test, the Anderson-Darling (A-D) test and the Chi-Squared ( $X^2$ ) test. The three tests compare the normalized data with an assumed statistical distribution (normal distribution in this case) using a critical value  $\alpha$  that defines the sensitivity of the tests and hence specifies the significance levels at which the hypothesis might be rejected. For example, an  $\alpha$  value of 0.01 implies that the hypothesis is rejected 1% of the time. The test was passed for all the critical values as shown in Table 6 and Table 7 for single and double lap joints respectively. These tables also report a statistic value which defines the likelihood of the hypothesis being rejected, with rejection being less likely as the value approaches zero. The statistic values for the A-D and K-S tests were close to zero, while the value for the  $X^2$  test digressed farther from zero. The tests also specify a p-value which provides the probability of the data fitting the assumed statistical distribution. For example, a p-value of 1 represents a 100% probability that the data fits the normal distribution. The p-value of the K-S test was closer to 1 as compared to the  $X^2$  test (the A-D test does not provide a p-value). Overall, the data passed all the three normality tests with a good correlation between the data set and a normal distribution for both single and double lap joints. More information on normality testing can be found in the literature [34,35].

With the normality of the data set verified, the 95 percentile and 99.87 percentile equations were obtained by using the same data fitting method as for Eqs. (7)–(10). However, the debonding load was substituted by ‘debonding load minus 1.645 times the standard deviation’ for the 95 percentile equations and by ‘debonding load minus 3 times the standard deviation’ for the 99.87 percentile equations. Consequently, the 99.87 and 95 percentile equations for both fracture energy and modified Adams model are specified below.

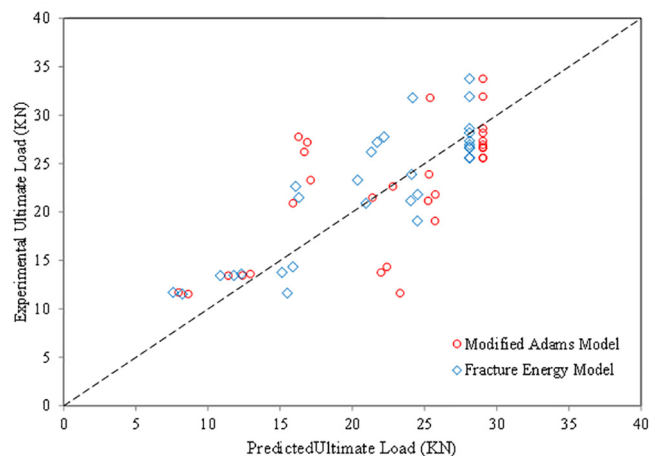


Fig. 9. Comparison between experimental and predicted results for Fracture energy and Modified Adams model.

**Table 4**  
Standard deviation (SD) and coefficient of variation (CoV) among specimens grouped by bond lengths.

Bond length (mm)	Single lap joints			Double lap joints			
	$\bar{F}$ (kN)	SD (kN)	CoV (%)	Bond length (mm)	$\bar{F}$ (kN)	SD (kN)	CoV (%)
25	2.0	12.1	16.4	10	14.5	1.9	13.0
37.5	4.4	16.8	26.4	25	19.2	1.7	9.1
50	2.6	25.1	10.3	50	31.1	1.7	5.3
62.5	4.4	23.5	18.7	75	51.4	5.3	10.3
75	2.9	28.0	10.5	100	54.6	3.1	5.7
100	2.1	28.2	7.5				

**Table 5**  
Normalized test data.

Specimen	Single lap joints		Double lap joints		
	Failure load (kN)	Normalized debonding load	Specimen	Failure load (kN)	Normalized debonding load
1S25a	11.5	0.91	2S 10a	14.0	0.97
1S25b	11.7	0.92	2S 10b	16.6	1.15
1S25c	13.5	1.06	2S 10c	16.8	1.16
1S25d	13.6	1.07	2S 10d	12.5	0.86
1S25e	13.4	1.05	2S 10e	12.5	0.86
1S37.5a	21.5	1.28	2S 25a	17.5	0.91
1S37.5b	11.6	0.69	2S 25b	18.7	0.97
1S37.5c	13.8	0.82	2S 25c	20.7	1.08
1S37.5d	22.6	1.35	2S 25d	17.4	0.91
1S37.5e	14.3	0.85	2S 25e	21.8	1.13
1S50a	23.3	0.93	2S 50a	31.1	1.00
1S50b	27.8	1.11	2S 50b	30.0	0.96
1S50c	20.9	0.83	2S 50c	29.6	0.95
1S50d	27.2	1.08	2S 50d	34.2	1.10
1S50e	26.2	1.04	2S 50e	30.6	0.98
1S62.5a	21.8	0.93	2S 75a	50.6	0.98
1S62.5b	31.8	1.35	2S 75b	59.0	1.15
1S62.5c	19.1	0.81	2S 75c	45.2	0.88
1S62.5d	21.1	0.90	2S 75d	55.8	1.09
1S62.5e	23.9	1.01	2S 75e	46.6	0.91
1S75a	26.7	0.95	2S 100a	48.8	0.89
1S75b	27.3	0.98	2S 100b	55.0	1.01
1S75c	25.6	0.91	2S 100c	55.0	1.01
1S75d	26.6	0.95	2S 100d	57.9	1.06
1S75e	33.8	1.21	2S 100e	56.6	1.04
1S100a	28.2	1.00			
1S100b	25.6	0.91			
1S100c	31.9	1.13			
1S100d	28.6	1.01			
1S100e	27.0	0.95			

4.5. Fracture energy model

The final 99.87 and 95 percentile equations for the fracture energy model were obtained by recalculating the calibration factors ( $C_{c1}$  and  $C_{c2}$  in Eqs. (7) and (8)) according to the reduced debonding loads. The

**Table 6**  
Statistical values from the normality tests for single lap joints.

Test	Statistic	P-value	Critical value				
			0.2	0.1	0.05	0.02	0.01
K-S	0.126	0.678	0.19 < <b>1.07</b>	0.22 < <b>1.22</b>	0.24 < <b>1.36</b>	0.27 < <b>1.51</b>	0.29 < <b>1.63</b>
A-D	0.603	–	1.37 > <b>1.29</b>	1.94 > <b>1.93</b>	2.50 > <b>2.49</b>	3.29 > <b>3.07</b>	3.90 > <b>3.86</b>
$\chi^2$	3.812	0.282	<b>4.64</b>	<b>6.25</b>	<b>7.81</b>	<b>9.84</b>	<b>11.34</b>

\*Six degrees of freedom used in  $\chi^2$  test.

Bold numbers are threshold for hypothesis to pass the normality test.

general form of the FRP-to-FRP debonding critical length and bond capacity expression according to the fracture energy model as discussed in Section 4.1 and described by Eqs. (7) and (8) were recalibrated using the non-linear least squares curve fitting method with 95% confidence bounds as described previously. The summary of all the calibration coefficients for 99 and 99.87 percentile equations for both single and double lap joints are reported in Table 8. Incorporating the coefficients from Table 8 into Eqs. (7) and (8) gives the 95 and 99.87 percentile equations for both single and double lap joints.

4.6. Modified Adams model

The final 99.87 and 95 percentile equations for the fracture energy model were obtained by recalculating the calibration factors ( $C_{c3}$  and  $C_{c4}$ ) in Eqs. (14) and (15), from the design equations for the Adams modified model as discussed in Section 4.2. The general form of these equations is given by Eqs. (14) and (15). Similar to the fracture Energy model, the equations from the Adams modified model were also recalibrated according to the reduced debonding loads to calculate the calibration coefficients ( $C_{c3}$  and  $C_{c4}$ ). The coefficients, reported in Table 9, can be incorporated into Eqs. (14) and (15) to obtain the 95 and 99.87 percentile equations for the modified Adams model.

The effectiveness of the equations was verified by plotting the Q-Q plots for single lap joints in Fig. 10 and Fig. 11. Almost all the data points were above the dotted line, which indicates that the predicted loads were reduced by a certain degree when compared to the Q-Q plots for the average models and hence make the 99.87 and 95 percentile equations more reliable to be used by engineers for design purposes.

5. Conclusions and recommendations

A comprehensive characterization of FRP-to-FRP bond behavior was compiled using a set of small scale experiments. The main conclusions have been summarised below:

1. The existence of an effective lap length has been confirmed for FRP-to-FRP bond connections, beyond which there is no increase in the debonding load, as can be seen in Fig. 5. The existence of an effective lap length was previously observed in FRP-to-concrete bond connections, but it has never been reported for FRP-to-FRP bond connections. Contrarily to FRP-to-concrete bond connections, the increase of lap length in FRP-to-FRP connections does not increase the ductility of the connection.
2. Two theoretical models were developed and further calibrated with the available experimental data, one being more accurate than another but the latter being simpler than the former. Lower bound characteristic equations were also reported.
3. Shear strength of commercially available resins is not typically given by manufacturers and distributors but is the primary failure mode in the FRP-to-FRP joints. It would be advisable that manufacturers specify shear strength values of resins obtained using standard tests.
4. Typical straight coupons were used in the research, while one of the most common uses of FRP-to-FRP bond connections is the use of FRP anchors. The behavior of the bond connection between the anchor

**Table 7**  
Statistical values from the normality tests for double lap joints.

Test	Statistic	P-value	Critical value				
			0.2	0.1	0.05	0.02	0.01
K-S	0.126	0.678	0.19 < <b>1.07</b>	0.22 < <b>1.22</b>	0.24 < <b>1.36</b>	0.27 < <b>1.51</b>	0.29 < <b>1.63</b>
A-D	0.679	–	1.37 > <b>1.29</b>	1.94 > <b>1.93</b>	2.50 > <b>2.49</b>	3.29 > <b>3.07</b>	3.90 > <b>3.86</b>
$\chi^2$	3.813	0.282	<b>4.64</b>	<b>6.25</b>	<b>7.81</b>	<b>9.84</b>	<b>11.34</b>

\*Six degrees of freedom used in  $\chi^2$  test.  
Bold numbers are threshold for hypothesis to pass the normality test.

**Table 8**  
Calibration coefficients for 95 and 99.87 percentile equations.

Single lap joints				Double lap joints			
$N_{bond}^{95\%}$		$N_{bond}^{99.87\%}$		$N_{bond}^{95\%}$		$N_{bond}^{99.87\%}$	
$C_{c1}$	$C_{c2}$	$C_{c1}$	$C_{c2}$	$C_{c1}$	$C_{c2}$	$C_{c1}$	$C_{c2}$
0.30	0.24	0.30	0.28	0.20	0.52	0.20	0.57

**Table 9**  
Calibration coefficients for 95 and 99.87 percentile equations for the modified Adams model

Single lap joints				Double lap joints			
$N_{bond}^{95\%}$		$N_{bond}^{99.87\%}$		$N_{bond}^{95\%}$		$N_{bond}^{99.87\%}$	
$C_{c3}$	$C_{c4}$	$C_{c3}$	$C_{c4}$	$C_{c3}$	$C_{c4}$	$C_{c3}$	$C_{c4}$
0.27	0.42	0.33	0.50	0.40	0.80	0.50	1.00

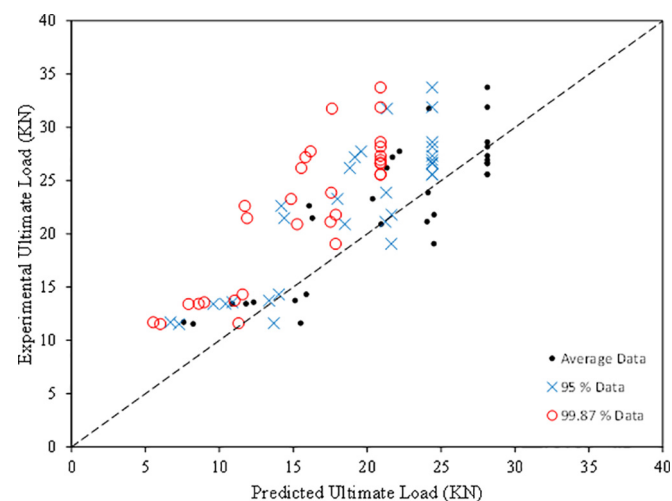


**Fig. 10.** Q-Q plot for Fracture energy model.

splay and the FRP substrate might be different to that observed in this study, and further research needs to be undertaken to verify the behavior of anchor splays.

**Acknowledgements**

The assistance provided by the lab technicians and personnel of the Department of Civil and Environmental Engineering at University of Auckland was essential in completion of the reported project. The authors thank Sika (NZ) for supplying the necessary materials required for the reported project.

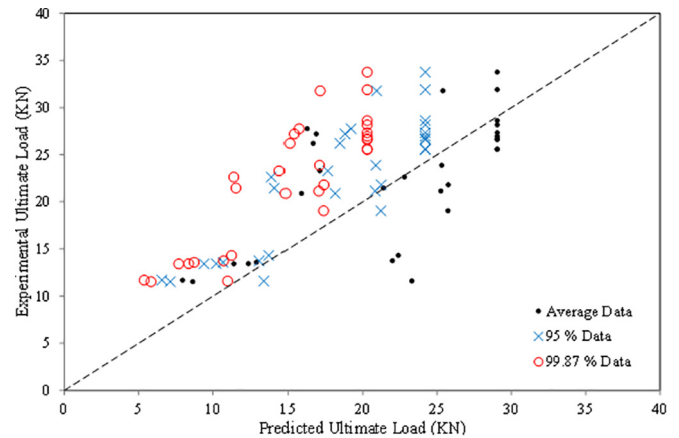


**Fig. 11.** Q-Q plot for Modified Adams model.

**Appendix A. Supplementary data**

Supplementary data associated with this article can be found, in the online version, at <https://doi.org/10.1016/j.compstruct.2018.12.005>.

**References**

- [1] Lam L, Teng J. Strength of RC cantilever slabs bonded with GFRP strips. *J Compos Constr* 2001;5(4):221–7. URL: [http://ascelibrary.org/doi/abs/10.1061/\(ASCE\)1090-0268\(2001\)5:4\(221\)](http://ascelibrary.org/doi/abs/10.1061/(ASCE)1090-0268(2001)5:4(221)).
- [2] Kalfat R, Al-mahaidi R, Smith ST. Anchorage devices used to improve the performance of reinforced concrete beams retrofitted with FRP composites: state-of-the-art review. *J Compos Constr* 2013;17(1):14–33. [https://doi.org/10.1061/\(ASCE\)CC.1943-5614.0000276](https://doi.org/10.1061/(ASCE)CC.1943-5614.0000276).
- [3] del Rey Castillo E, Dizhur D, Griffith MC, Ingham JM. Strengthening RC structures using FRP spike anchors in combination with EBR systems. *Compos Struct* 2019. <https://doi.org/10.1016/j.compstruct.2018.10.093>.
- [4] E. del Rey Castillo, M.C. Griffith, J.M. Ingham, FRP anchors attributes, University of Auckland, 10.17608/k6.auckland.5188456, 2017.
- [5] Kim SJ, Smith ST. Pullout Strength Models for FRP Anchors in Uncracked Concrete. *J Compos Constr* 2010;14(4):406–14. [https://doi.org/10.1061/\(ASCE\)CC.1943-5614.0000097](https://doi.org/10.1061/(ASCE)CC.1943-5614.0000097).
- [6] Villanueva Llauradó P, Ibell T, Fernández Gómez J, González Ramos FJ. Pull-out and shear-strength models for FRP spike anchors. *Compos Part B: Eng* 2017;116:239–52. <https://doi.org/10.1016/j.compositesb.2017.02.029>.
- [7] del Rey Castillo E, Griffith MC, Ingham JM. Straight FRP anchors exhibiting fiber rupture failure mode. *Compos Struct* 2019;207:612–24.
- [8] Park YB, Song MG, Kim JJ, Kweon JH, Choi JH. Strength of carbon/epoxy composite single-lap bonded joints in various environmental conditions. *Compos Struct* 2010;92(9):2173–80. <https://doi.org/10.1016/j.compstruct.2009.09.009>.
- [9] Cree D, Gamaniouk T, Loong ML, Green MF. Tensile and lap-splice shear strength properties of CFRP composites at high temperatures. *J Compos Constr* 2015;19(2):1–12. [https://doi.org/10.1061/\(ASCE\)CC.1943-5614.0000508](https://doi.org/10.1061/(ASCE)CC.1943-5614.0000508).
- [10] Volkersen O. Rivet strength distribution in tensile-stressed rivet joints with constant cross-section. *Luftfahrtforschung* 1938;15(1):41–7.
- [11] Allman DJ. A theory for elastic stresses in adhesive bonded lap joints. *Q J Mech Appl Math* 1977;30(4):415–36.
- [12] Kaniatkar R, Smith ST, Lewis C. An Experimental Investigation on the splay angle of embedded FRP tension anchors. Proceedings of The 8th International Conference on Fibre-Reinforced Polymer (FRP) Composites in Civil Engineering (CICE 2016) Hong Kong, China: Department of Civil and Environmental Engineering & Research Institute for Sustainable Urban Development, The Hong Kong Polytechnic University; 2016. p. 413–8.
- [13] Chen J, Teng J. Anchorage strength models for FRP and steel plates bonded to

- concrete. *J Struct Eng* 2001;127(7):784–91.
- [14] ACI 440.2R, Guide for the Design and Construction of Externally Bonded FRP Systems for Strengthening Concrete Structures, American Concrete Institute (ACI) Committee 440, Farming Hills, Michigan, U.S.A, 2017. doi: 10.1061/40753(171)159. URL: <http://www.afzir.com/sites/default/files/kb/attached/3.pdf>.
- [15] CNR-DT 200, Guide for the Design and Construction of Externally Bonded FRP Systems for Strengthening Existing Structures, CNR (Consiglio Nazionale delle Ricerche) – Advisory Committee on Technical Recommendations for Construction, Rome, Italy, 2013.
- [16] del Rey Castillo E, Griffith M, Ingham J. Seismic behavior of RC columns flexurally strengthened with FRP sheets and FRP anchors. *Compos Struct* 2018;203:382–95. <https://doi.org/10.1016/j.compstruct.2018.07.029>.
- [17] SIKA, SikaWrap 600 C Product Data Sheet, SIKA (NZ) Ltd., Auckland, New Zealand, 2013.
- [18] SIKA, Sikadur 300 Product Data Sheet, SIKA (NZ) Ltd., Auckland, New Zealand, 2013.
- [19] ASTM D3039, Standard Test Method for Tensile Properties of Polymer Matrix Composite Materials, American Society for Testing and Materials (ASTM), West Conshohocken, Pennsylvania, 2014. doi: 10.1520/D3039\_D3039M-14.
- [20] ASTM D790, Standard Test Methods for Flexural Properties of Unreinforced and Reinforced Plastics and Electrical Insulating Materials, American Society for Testing and Materials (ASTM), West Conshohocken, Pennsylvania, 2017.
- [21] ASTM D638, Standard Test Method for Tensile Properties of Plastics, American Society for Testing and Materials (ASTM), West Conshohocken, Pennsylvania, 2014. doi:10.1520/D0638-14.1.
- [22] ASTM D5868, Standard Test Method for Lap Shear Adhesion for Fiber Reinforced Plastic ( FRP ), American Society for Testing and Materials (ASTM), 2014. doi:10.1520/D5868-01R14.2.
- [23] ASTM D3528, Standard Test Method for Strength Properties of Double Lap Shear Adhesive Joints by, American Society for Testing and Materials (ASTM), 2016. doi:10.1520/D3528-96R16.2.
- [24] ASTM D5868, Standard Test Method for Lap Shear Adhesion for Fiber Reinforced Plastic ( FRP ), American Society for Testing and Materials (ASTM), 2014. doi:10.1520/D5868-01R14.2.
- [25] MATLAB, MATLAB and Statistics Toolbox Release 2015. The MathWorks Inc., Natick, Massachusetts, United States; 2015.
- [26] Stubbing RM. Characterisation of polymeric foam cores using digital image correlation. *The University of Auckland, Department of Mechanical Engineering*; 2013. [Ph.D. thesis].
- [27] Stubbing RM, DTA Report 408/NR 1690 – Digital Image Correlation Capability, Defence Technology Agency (DTA), New Zealand Defence Force. <http://www.dta.mil.nz/wp-content/uploads/Report408.pdf>, Auckland, New Zealand, 2016.
- [28] da Silva LFM, das Neves PJC, Adams RD, Wang A, Spelt JK. Analytical models of adhesively bonded joints-Part II: Comparative study. *Int J Adhesion Adhesives* 2009;29(3):331–41. <https://doi.org/10.1016/j.ijadhadh.2008.06.007>.
- [29] Adams RD, Mallick V. A method for the stress analysis of lap joints. *J Adhesion* 1992;38(3–4):199–217. <https://doi.org/10.1080/00218469208030455>.
- [30] Holzenkämpfer P, Ingenieurmodelle des verbunds geklebter bewehrung für betonbauteile, no. 473 Edition; 1997.
- [31] Outwater, J, Murphy, MC, The fracture energy of composite materials Final report, 1 Sep. 1967–31 Aug. 1968 (Fracture energy of composite materials) (September).
- [32] Adams R, Wake W. *Structural adhesive joints in engineering*. Springer Science & Business Media; 1997.
- [33] Goland M, Reissner E. The stresses in cemented joints. *J Appl Mech* 1944;11(1):A17–27.
- [34] D'Agostino RB, Tests for the Normal Distribution, in: D'Agostino, R.B.; Stephens, M. A. Goodness-of-fit Techniques, Marcel Dekker. ISBN 0-8247-7487-6, New York, USA; 1986.
- [35] Thode Jr. HC. *Testing for normality*. New York, USA: Marcel Dekker; 2002. ISBN 8247-9613-6.